

# GalRotpy: a tool to parametrize the gravitational potential of disc-like galaxies<sup>☆</sup>

Andrés Granados<sup>\*,a,b</sup>, Daniel Torres<sup>b</sup>, Leonardo Castañeda<sup>b</sup>, Lady Henao<sup>c</sup>, Santiago Vanegas<sup>b</sup>

<sup>a</sup> Departamento de Física, Universidad Nacional de Colombia, Carrera 30 Calle 45-03, P.A. 111321 Bogotá, Colombia

<sup>b</sup> Observatorio Astronómico Nacional, Universidad Nacional de Colombia, Carrera 30 Calle 45-03, P.A. 111321 Bogotá, Colombia

<sup>c</sup> Departamento de Astronomía, Universidad de Concepción, Avenida Esteban Iturra s/n. Castilla 160-C Concepción, Chile

## ABSTRACT

**GalRotpy** is a Python3-based tool, intended to determine the contribution of each mass component to the gravitational potential of disc-like galaxies by means of their rotation curve. Besides, **GalRotpy** allows to perform a parametric fit of a given rotation curve, which relies on a MCMC procedure implemented by using `emcee` package. Here the gravitational potential of disc-like galaxies is built from the contribution of a Miyamoto-Nagai potential model for the bulge/core and the thin/thick disc, an exponential disc, together with the NFW (Navarro-Frenk-White) potential or the Burkert (cored density profile) potential for the Dark Matter halo, where each contribution is implemented by using `galpy` package. We summarize the properties of each contribution to the rotation curve involved, and then describe how **GalRotpy** is implemented along with its capabilities. Finally we present the characterization of two galaxies, NGC6361 and M33, and show that the results for M33 provided by **GalRotpy** are consistent with those found in the literature.

## 1. Introduction

In 1914 Vesto Slipher discovered that spiral galaxies rotate, by detecting inclined absorption lines in nuclear spectra from M31 and Sombrero galaxies [Slipher \(1914\)](#). Later, Jan Oort in 1932, first found that there must be three times as much mass as it is observed in visible light when he studied stellar motions above the galactic plane. This finding prompted him to include undetected components like interstellar medium to explain the missing mass. Similar observations for the external parts of NGC3115 galaxy, showed that the mass-to-light ratio is about two orders of magnitude larger than in the solar neighborhood [Oort \(1940\)](#), as evidence of no visible matter. The latter is known as the *missing mass* problem; it is, the mass contained in the bright objects of a defined region in space does not correspond to its dynamical mass, brought to us by its gravitational interactions.

The mass-to-light ratio  $Y = M/L$  is a quantity that describes how much the mass is a fraction of the light expressed in solar units ( $Y_{\odot} = M_{\odot}/L_{\odot}$ ). It has been the main tool for investigating the *missing mass* problem in stellar systems like the Milky Way galaxy, external galaxies, and cluster of galaxies.

It has been raised some explanations concerning the *missing mass* problem. H. Babcock in 1939 found that the rotation curve is approximately flat on the periphery of M31 galaxy, instead of the expected Keplerian decrease because of the diminishing in luminosity

(predicted by the luminous profile) [Babcock \(1939\)](#). He concluded that the mass-to-light ratio must be not constant in the galactic radius, but it must increase. He suggested two explanations for this phenomenon: the light absorption must increase in external parts of the galaxy, or it is required a modification to the Newtonian dynamics [Sanders \(2010\)](#).

The findings published by Fritz Zwicky [Zwicky \(1933, 1937\)](#), suggested the existence of some sort of *unseen matter* or dark matter in his results using the virial theorem applied to the velocities of galaxies in the Coma galaxy cluster. Zwicky measured the radial velocities of the galaxies in the cluster, and thus he estimated the cluster mass as well as the average galaxy mass. Then comparing this value with the luminosity, he obtained the mass-to-light ratio for galaxies in the cluster  $Y = 500Y_{\odot}$  suggesting that the major contribution comes from dark matter in the cluster. Later, in 1970 Vera Rubin, first reveals an observational evidence of dark matter in M31 galaxy. She realized the flattened circular velocity in the external regions of the galaxy based on the galaxy rotation curve from 67 Hii spectra within a range in the galactic radius of  $(3 - 24 \text{ kpc})$  [Rubin and Ford Jr \(1970\)](#).

The rotation curve of disc-like galaxies is the main kinematic observable data that allow the study of dynamical properties of its stars and interstellar gas, in addition to structure, evolutionary and formation processes of the galaxy [Sofue and Rubin \(2001\)](#). The shape of rotation curves was related to the morphology of spiral galaxies [Rubin et al. \(1980\)](#) looking for a universal rotation curve depending

\* <https://github.com/andresGranadosC/GalRotpy.git>

<sup>☆</sup> Corresponding author.

E-mail addresses: [a.granadosc@unal.edu.co](mailto:a.granadosc@unal.edu.co) (A. Granados), [daatorresba@unal.edu.co](mailto:daatorresba@unal.edu.co) (D. Torres), [lcastanedac@unal.edu.co](mailto:lcastanedac@unal.edu.co) (L. Castañeda), [lhenao@astro-udec.cl](mailto:lhenao@astro-udec.cl) (L. Henao), [svanegasp@unal.edu.co](mailto:svanegasp@unal.edu.co) (S. Vanegas).

only on the galaxy luminosity Persic et al. (1996), and not only on the luminosity but by a multi-parameter family such as morphological type, the shape of the light distribution and other optical properties Noordermeer et al. (2007).

The mass distribution in a component of a galaxy can be estimated by the assumption that the mass-to-light ratio is constant Binney and Tremaine (2011). Given that the galaxy luminosity is an astrophysical observable, it can be obtained a light profile of a galaxy component and, therefore to infer its mass distribution. Then, it is possible to find the rotation curve for each mass contribution and derive interesting quantities like bulge to disc or bulge to the dark matter halo mass ratios, or equally interesting the radial extension of each mass component. The modeling of a rotation curve using mass decomposition is widely used even in recent studies, since it evidences the influence of all the mass contributions in each position.

Following the method of mass decomposition, **GalRotpy** is intended to visualize the parametric building of a rotation curve of disc-like galaxies in its main mass constituents and then to make an estimation of the parameters and their uncertainties associated to each contribution. A rotation curve can be fitted by changing in real time two or more gravitational potential parameters, to give a first glance about the importance of the different mass components of a galaxy, that can be compared directly with observational data. Therefore **GalRotpy** is also presented as a teaching guide for gravitational potential theory and dynamics of galaxies.

This paper is arranged in the following way. In section 2 we summarize the theory of gravitational potential as the foundations of **GalRotpy**, where we focus on the functional form of four gravitational potentials used to model the galaxy's mass components and their circular velocities: Miyamoto-Nagai for the bulge and thin/thick disc, the exponential disc and the Navarro-Frenk-White or Burkert for the dark matter halo. Here, we also make a brief discussion on how this decomposition has been implemented Sofue (1996, 2016); Pouliasis et al. (2017), which is a reference for defining the input parameters used in **GalRotpy**. This is followed by section 3, in which we give the outline of how **GalRotpy** is implemented and how it works. Continuing with section 4, it is presented the application of **GalRotpy** to two spiral galaxies, NGC6361 and M33, in order to estimate the potential parameters like mass (or density), galactocentric distance and height scales from the rotation curve. Finally, the conclusions and summary are subject of section 5.

## 2. Gravitational potential of disc-like galaxies

In this section we take into account the primary results on the theory of gravitational potential related to different mass components in disc-like galaxies Fig. 1; we also show the equations of circular

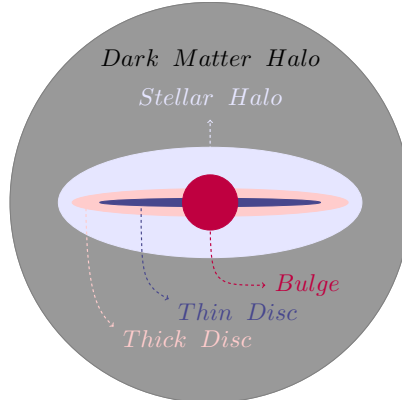


**Fig. 1.** Diagram of the main components of disc-like galaxies: spheroidal bulge, thin and thick discs, spheroidal stellar and Dark Matter halos.

velocity and the meaning of the parameters for these potentials to understand the basis to decompose the observed rotation curve of disc galaxies. The potential theory is the fundamental issue needed to extract the kinematical features from rotation curves, and deduce the dynamics of these systems.

### 2.1. Potential Theory

A galaxy is a system of stars, interstellar gas and dark matter that interact between them fundamentally following Newton's theory of gravity. The whole mass of a disc-like galaxy is composed of different masses associated with its constituents stellar systems. The mass distributions will give us the functional form for the potentials according to the Newton gravity law expressed in its differential form by Poisson's equation Samurovic (2007); Binney and Tremaine (2011):

$$\nabla^2 \Phi(\mathbf{x}) = 4\pi G \rho(\mathbf{x}), \quad (1)$$

with  $G$  the gravitational constant,  $\rho$  the mass density of the given system and  $\Phi(\mathbf{x})$  the gravitational potential this systems generates. From now on we will refer to  $\Phi = \Phi(\mathbf{x})$  as potential.

The Poisson's equation equation (1) is an elliptical partial differential equation that allows linearity. It means that if two sources with mass density  $\rho_1$  and  $\rho_2$  generate the potentials  $\Phi_1$ , and  $\Phi_2$  respectively, then the source with mass density  $\rho = \rho_1 + \rho_2$  generates the potential  $\Phi = \Phi_1 + \Phi_2$ . Here linearity is also known as the *superposition principle*, and it stays valid for as many mass components as needed. This is the key property implement in **GalRotpy** tool, since it allows the decomposition of the total potential of a given galaxy into its different components, and thus use them separately.

When we can set  $\Phi(\mathbf{x} \rightarrow \infty) = 0$  the solution to (1) is

$$\Phi(\mathbf{x}) = -G \int d^3x' \frac{\rho(\mathbf{x}')}{|\mathbf{x}-\mathbf{x}'|}, \quad (2)$$

where the integral is taken over all the mass distribution, such that (2) satisfies  $\mathbf{F} = -\nabla\Phi$ , with  $\mathbf{F}$  being the total force per unit mass on a particle, also known as the gravitational field.

For a deep discussion on potential theory in the gravitational context refer to Binney and Tremaine (2011).

### 2.2. Circular velocity

The central issue of this work is to compute the circular velocity  $V_c$  (in the equatorial plane) associated to a gravitational potential  $\Phi(R, z = 0)$  of a disc-like galaxy, which is described by

$$V_c^2(R) = R \frac{\partial \Phi}{\partial R}, \quad (3)$$

where in case of a spherical symmetric distribution, this velocity is not fixed at the equatorial plane, and reads

$$V_c^2 = \frac{G}{R} M(\leq R), \quad (4)$$

Thus, along to the linearity of Poisson's equation (1), we have that, for a system composed by  $n$  mass distributions, it is characterized by the gravitational potential

$$\Phi = \Phi_T = \sum_i^n \Phi_i, \quad (5)$$

such that, according to equation (3) and the potentials composition (5), the total circular velocity reads

$$V_c^2 = \sum_i^n V_{c(i)}^2. \quad (6)$$

Therefore, using equation (3), we obtain the circular velocities associated to each potential that we will use to model the rotation curve equation (6) of a disc-like galaxy Binney and Tremaine (2011).

### 2.3. Potentials of a disc-like galaxy

It is a tough task to resolve the Poisson equation for  $\Phi(\mathbf{x})$  given a mass density  $\rho(\mathbf{x})$ . However, supported by symmetry considerations and observed luminosity profiles it is possible to simplify the problem and to find a functional form for the mass distribution of a spiral galaxy [Miyamoto and Nagai \(1975\)](#).

There are different combinations of potentials which permit to characterize the rotation curve of a given disc galaxy, for example in [Sofue \(1996\)](#) the rotation curve for the Milky Way galaxy was modeled using the Miyamoto-Nagai potential for four different components, while in [Pouliasis et al. \(2017\)](#) for this very same rotation curve, two models are given, where Miyamoto-Nagai potential, Plummer potential and a truncated spherical symmetric potential are used to model the thin/thick disc, the bulge and the dark halo respectively. In this way, [Sofue \(2016\)](#) modeled the rotation curve of several disc galaxies by means of the de Vaucouleurs potential for the bulge, an exponential disc and a NFW dark halo. Besides, it has been shown that Burkert cored distribution is useful to describe the dark halo for dwarf galaxies for example (see [Karukes and Salucci \(2016\)](#)).

Therefore, we have a guide of what potentials (mass distributions) are the best to be include in **GalRotpy**, taking into account that we will use **galpy** to implement the different contributions of a given rotation curve. Thus, as a first approximation to the real dynamics of disc-like galaxies, **GalRotpy** uses calculations of two axisymmetric potentials to model the barionic matter component, while it uses two spherical symmetric potentials to model the dark matter component. The mass distribution of a disc galaxy can be decomposed mainly into three mass components: bulge, disc, and Dark Matter Halo [Sofue \(2016\)](#). Below, we present in context the historical development of these components, the functional forms for its gravitational potentials and its importance in the understanding of the rotation curve of disc-like galaxies.

For the distributions that follow, we have that  $r$  represents the spherical radius, while the pair  $R$  and  $z$  represent the cylindrical coordinates. Here  $R$  is the galactocentric distance.

#### 2.3.1. Miyamoto-Nagai potential

The Miyamoto - Nagai potential [Miyamoto and Nagai \(1975\)](#) is an axisymmetric potential used to model the bulge and the thin/thick disc of a galaxy. The given potential is defined as

$$\Phi_{MN}(R, z) = -\frac{GM}{\sqrt{R^2 + (a + \sqrt{z^2 + b^2})^2}}, \quad (7)$$

with the free parameters  $a$ ,  $b$ , and  $M$  being the length, height scales and total mass of the distribution. Thus, for this potential its associated circular velocity [equation \(8\)](#) reads

$$V_c(R) = R \sqrt{\frac{GM}{(R^2 + (a + b)^2)^{3/2}}}. \quad (8)$$

The [Fig. 2](#) represents the changes in the rotation curve's shape by three values of amplitude. These values are traced by the quantity  $M$  (top) representing the mass in the Miyamoto-Nagai model and the height scale  $b$  (bottom) that determines the flatness of the mass density (better traced by the dimensionless scale ratio  $b/a$ ). The model (7) is free of singularities and tends to the Newtonian point mass potential when  $R$  and  $z$  become large [Miyamoto and Nagai \(1975\)](#).

This potential is a generalization of the Plummer potential ( $a = 0$ ) [Plummer \(1911\)](#) and Kuzmin potential ( $b = 0$ ) [Kuzmin \(1956\)](#), also known as Toomre's model 1 [Toomre \(1963\)](#). These potentials are intended to model respectively thin discs and globular clusters. Refer to [Binney and Tremaine \(2011\)](#) for further details.

#### 2.3.2. Razor thin exponential disc potential

It has been found that for many disc galaxies their surface brightness outside the inner region (where the disc is the dominant baryonic

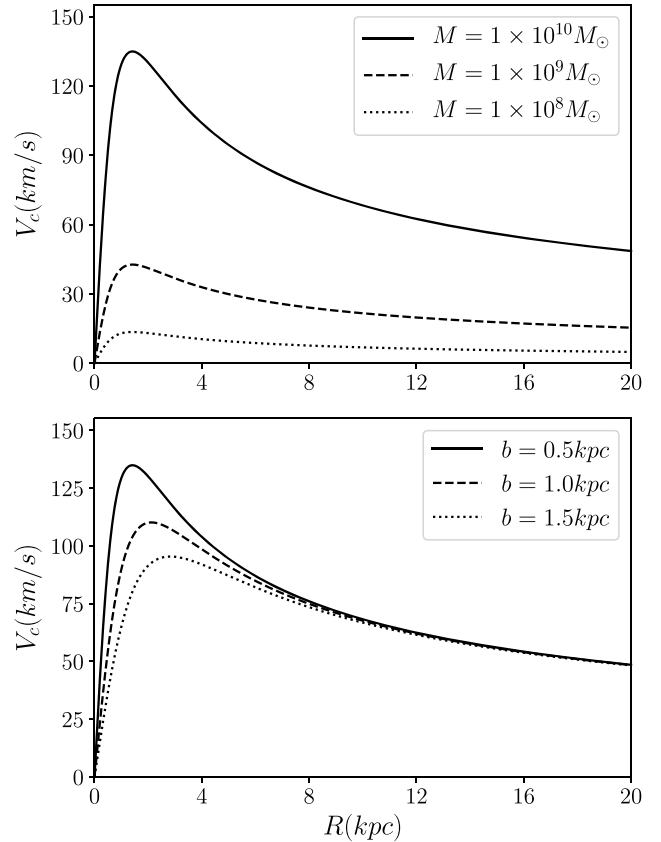


**Fig. 2.** Rotation curve for the Miyamoto-Nagai potential with three values of the amplitude  $M$  (top) and the scale parameter  $b$  (bottom).

component) is represented by an exponential profile [Binney and Tremaine \(2011\); Mo et al. \(2010\)](#). From this property it was inferred by [Freeman \(1970\)](#) that the mass density of a disc can be written as

$$\rho_d(R) = \Sigma_0 \exp(-R/h_r) \delta(z), \quad (9)$$

which is known as an exponential disc. Here the free parameters  $\Sigma_0$  and  $h_r$  are the central surface mass density and the radial scale, respectively. Meanwhile,  $\delta(z)$  is the Dirac's delta function.

For this distribution the gravitational potential derived from (9), and evaluated in the equatorial plane reads

$$\Phi_{ED}(R, 0) = -\pi G \Sigma_0 R (I_0(y) K_1(y) - I_1(y) K_0(y)), \quad (10)$$

with  $K_0$ ,  $K_1$  and  $I_0$ ,  $I_1$  being modified Bessel functions. This potential leads to the circular velocity

$$V_c(R) = \sqrt{4\pi G \Sigma_0 h_r y^2 (I_0(y) K_0(y) - I_1(y) K_1(y))}, \quad (11)$$

where  $y = R/2h_r$ . A detailed presentation of how (10) and (11) are derived can be found in [Binney and Tremaine \(2011\); Freeman \(1970\); Cuddeford \(1993\)](#). For this distribution the total mass of the disc is given in an straightforward manner from (9) as

$$M_d = 2\pi h_r^2 \Sigma_0. \quad (12)$$

Here, [Fig. 3](#) shows the change in the rotation curve shape by changes in the free parameters of [equation \(9\)](#). A change in surface density  $\Sigma_0$  represents from a very flat circular velocity up to a thick disc (top), and lower values in radius scale parameter  $h_r$  allows the reproduction of a thin disc.

#### 2.3.3. The Navarro-Frenk-White potential

Collisionless N-body numerical simulations of the clustering of dark matter particles suggest that the mass density within a Dark Matter halo has a similar structure to a power density model, and a universal scale

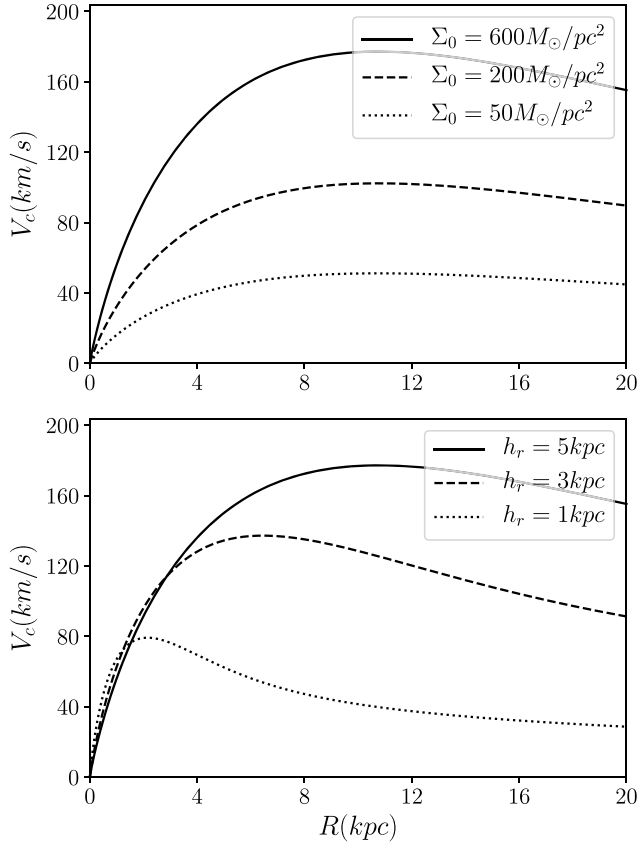


**Fig. 3.** Rotation curve for an exponential disc potential with three values of the central surface density  $\Sigma_0$  (top) and the scale parameter  $h_r$  (bottom).

behavior. It is interesting to see the similarity between the luminosity profile in elliptical galaxies Binney and Tremaine (2011) and the mass distribution in the Dark Matter halo. Such mass density is given by the two-power law

$$\rho(r) = \frac{\rho_0}{(r/a)^\alpha (1+r/a)^{\beta-\alpha}}. \quad (13)$$

In particular, for equation (13) with  $(\alpha, \beta) = (1, 3)$  it is called Navarro-Frenk-White (NFW) Navarro et al. (1997) density profile. This spherically symmetric profile has two free parameters, the scale radius  $a$  and the representative density  $\rho_0$  Navarro et al. (1997). Then, the corresponding gravitational potential for this density profile is

$$\Phi_{NFW}(r) = -\frac{GM_0}{r} \ln\left(1 + \frac{r}{a}\right), \quad (14)$$

with  $M_0 = 4\pi\rho_0 a^3$ . Such potential (14) leads to the circular velocity Binney and Tremaine (2011); Jimenez et al. (2003) in equation (15)

$$V_c(R) = \sqrt{\frac{GM_0}{R} \left[ \ln\left(1 + \frac{R}{a}\right) - \frac{R/a}{1+R/a} \right]}. \quad (15)$$

As it can be seen in Fig. 4, an increment in the quantity  $M_0$  results in greater amplitude and any change in scale parameter  $a$  gives a fast steep or larger coverage in the galactocentric distance of the galaxy. **Gal-Rotpy** works directly over the scale  $a$  and the effective mass  $M_0$  since it is the amplitude parameter implemented in `galpy`.

#### 2.3.4. The Burkert density profile

Cosmological simulations in the Cold Dark Matter (CDM) scenario predict halos with central density cusps that are not observed for several dwarfs, spirals and Low Mass Brightness (LMB) galaxies López Fune et al. (2017). The observed mass profiles of dwarf galaxies can be fitted by the phenomenological density distribution

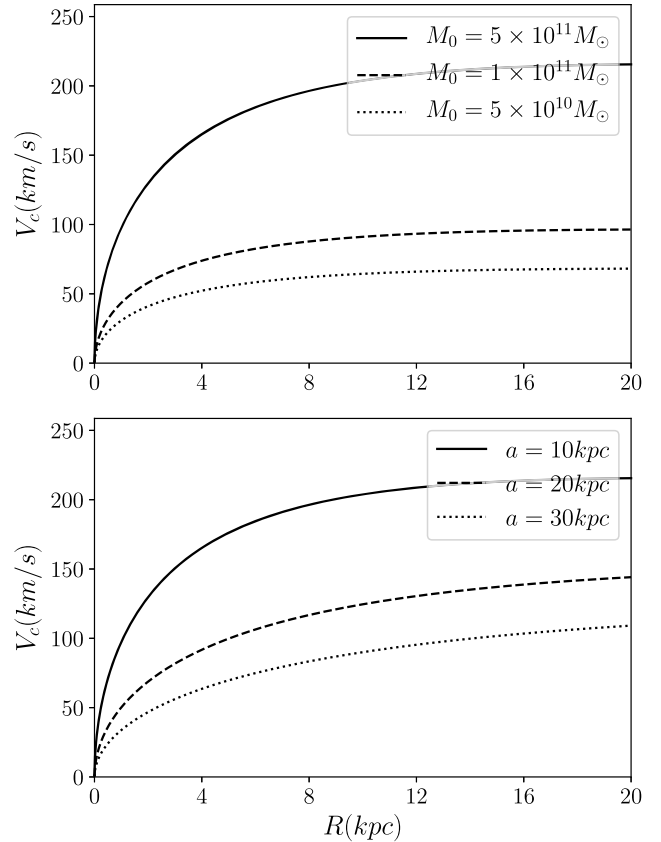


**Fig. 4.** Rotation curve for the Navarro-Frenk-White potential with three values of the amplitude  $M_0$  (top), and the radius scale parameter  $a$  (bottom).

Burkert (1995), known as the Burkert density profile, which is given by

$$\rho_{Bk}(r) = \frac{\rho_0 a^3}{(r+a)(r^2+a^2)}. \quad (16)$$

Here the free parameters  $\rho_0$  and  $a$  are the central core density and a scale radius, respectively.

This spherically symmetric density profile (16) leads to the potential

$$\Phi_{Bk}(r) = \pi G \rho_0 a^2 \left\{ \left(1 - \frac{a}{r}\right) \ln\left(1 + \frac{a}{r}\right) + \left(\frac{r}{a}\right)^2 + 2\left(1 + \frac{a}{r}\right) \left[ \tan^{-1}\left(\frac{r}{a}\right) - \ln\left(1 + \frac{r}{a}\right) \right] - \pi \right\}, \quad (17)$$

whose corresponding circular velocity turns out to be

$$V_c(R) = \sqrt{\frac{G\pi\rho_0 a^3}{R} \left[ 2 \ln\left(1 + \frac{R}{a}\right) + \ln\left(1 + \left(\frac{R}{a}\right)^2\right) - 2 \tan^{-1}\left(\frac{R}{a}\right) \right]}. \quad (18)$$

The given rotation curve is shown in Fig. 5, where a change in the density  $\rho_0$  (top) gives a specific value in the amplitude of the cored profile and a lower radius scale value  $a$  (bottom) results in a lower top velocity for the same central slope. An interesting property of this profile (17) is that, for practical purposes, it may be characterized by only one of the two parameters described above, since there is an approximate relation between  $a$  and  $\rho_0$  (see Burkert (1995); Salucci and Burkert (2000)), which states

$$\rho_0 \approx 4.5 \times 10^{-2} (a/\text{kpc})^{-2/3} M_\odot/\text{pc}^3. \quad (19)$$

Despite, this seems to be an advantage, we will work with  $a$  and  $\rho_0$  separately since equation (19) may induce biased results within the fitting process (see section 3.3). With respect to its implementation,

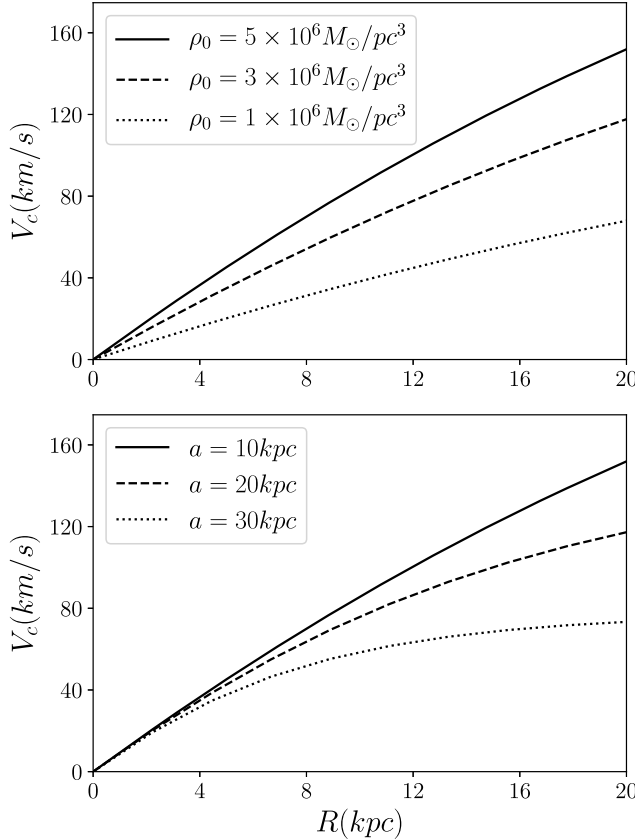


**Fig. 5.** Rotation curve for the Burkert potential with three values of the central core density  $\rho_0$  (top) and the radius scale parameter  $a$  (bottom).

unlike NFW profile, for Burkert profile `galpy` (and therefore also `GalRotpy`) uses as amplitude parameter  $\rho_0$  directly, and  $a$  as its scale factor [equation \(18\)](#).

### 2.3.5. Dark Halo's Mass

The intrinsic parameters of each distribution described above are the best ones to describe a given dark halo, nevertheless in the literature its total mass  $M_h$  is often used instead of the corresponding density  $\rho_0$ , which makes useful to give a brief description of how  $M_h$  is defined.

Theoretical work and computational simulations on gravitational collapse and cosmological structure formation have shown that the total mass (also known as critic mass) of a dark halo is well defined as the mass enclosed by a limiting radius  $r_c$ <sup>1</sup>, within which the mean mass density of the halo  $\bar{\rho}_h$  is given by [equation \(20\)](#)

$$\bar{\rho}_h = \Delta_c \rho_c, \quad (20)$$

such that

$$M_h = M(\leq r_c) = \frac{4\pi}{3} \bar{\rho}_h r_c^3 = \frac{4\pi}{3} \Delta_c \rho_c r_c^3. \quad (21)$$

Here  $\Delta_c$  is the critical overdensity and  $\rho_c$  is the cosmological critical mass density, with both being functions of the redshift  $z$  of the given galaxy, and also depend on the cosmology being used. In this work we make use of a flat  $\Lambda$ CDM universe with density parameters at redshift  $z = 0$  being  $\Omega_{m,0} = 0.3$  and  $\Omega_\Lambda = 0.7$  (in concordance with Planck collaboration [Ade et al. \(2016\)](#)), for which  $\Delta_c$  reads as in [equations \(22\)](#) and [\(23\)](#) [Bryan and Norman \(1998\)](#)

$$\Delta_c = 18\pi^2 + 82(\Omega_m - 1) - 39(\Omega_m - 1)^2, \quad (22)$$

<sup>1</sup> For the NFW and Burkert profiles, their mass  $M(\leq r)$  can be easily inferred from the corresponding circular velocity and [equation \(4\)](#).

where

$$\Omega_m = \frac{\Omega_{m,0}(1+z)^3}{\Omega_{m,0}(1+z)^3 + \Omega_\Lambda}. \quad (23)$$

Likewise, under the same cosmological paradigm,  $\rho_c$  can be written as in [equation \(24\)](#)

$$\rho_c = \frac{3H^2}{8\pi G} = \frac{3H_0^2}{8\pi G} \left( \Omega_{m,0}(1+z)^3 + \Omega_\Lambda \right), \quad (24)$$

with  $H_0 = 67.8 \text{ km s}^{-1} \text{ Mpc}^{-1}$  being the Hubble parameter at redshift  $z = 0$  [Ade et al. \(2016\)](#). It is worth mentioning that  $\Delta_c = 200$  [Navarro et al. \(1997\)](#) is often taken as a standard value. For a deeper discussion about this topic see for example [Mo et al. \(2010\)](#); [Navarro et al. \(1997\)](#); [Coe \(2010\)](#); [Bryan and Norman \(1998\)](#) and the references therein.

Now, it is clear from [\(21\)](#) that in order to obtain  $M_h$  we need  $r_c$ , which is obtained by solving [equation \(21\)](#) at a given  $z$  for a given profile and, its corresponding intrinsic parameters. In such way, defining the concentration parameter  $X := r_c/a$  the NFW profile leads to the equation

$$\frac{\Delta_c \rho_c}{3\rho_0} X^3 = \ln(1+X) - \frac{X}{1+X}, \quad (25)$$

while Burkert profile leads to the equation

$$\frac{4\Delta_c \rho_c}{3\rho_0} X^3 = 2\ln(1+X) + \ln(1+X^2) - 2\tan^{-1}(X). \quad (26)$$

Thus, solving for  $X$  we see that for both equations, non trivial real solutions have to be found numerically; plotting the function at both sides of the given equations [\(25\)](#) and [\(26\)](#) shows that there is only one non trivial real solution. Remember that the intrinsic parameters  $\rho_0$  and  $a$  are different for each profile.

### 3. GalRotpy

**GalRotpy** is a visual tool whose aim is to help to visualize and also to explore the rotation curve of disc-like galaxies considering the contribution of each component independently and as a whole, not only from a visual inspection but also through a parametric fit analysis.

In order to accomplish this task we make use of the following python packages to run **GalRotpy**: `matplotlib` to generate the interface and plots, `astropy` and `numpy` for units and array computations, `galpy` to construct the composed rotation curve, `emcee` to fit the data and obtain the most likely parameters by means of the MCMC procedure, and `corner` to plot the credible regions obtained from the fit process. Other packages are involved but not extensively used, then for a more detailed description about **GalRotpy**, see the repository page where the source code is available as well as its requirements and the instructions for its use.

#### 3.1. GalRotpy input

To run **GalRotpy** it is optional to give an initial set of mass components for having a first estimate of the gravitational potential parameters. There can be included a bulge and a dark matter halo, a disk and a halo or the three of them. If none of these options are included, **GalRotpy** will take a set of default estimates for each of the mass components (bulge, thin disc, thick disc, exponential disc, NFW-halo and burkert-halo). The parameters contains a value for the mass in  $M_\odot$  and, for the galactocentric distance and height scales in  $kpc$ , along with an associated threshold for each component.

The following potential parameters ([Table 1](#)) are based in those used to model the Milky Way galaxy and dwarf galaxies, which can be taken by default for a wide variety of galaxies.

On the other hand, the rotation curve must be introduced through a

**Table 1**

Set of parameters involved in each of the contributions considered in **GalRotpy**. The given range for each parameter attempts to be a guide about which values may be used to run this program, particularly for dwarf galaxies and Milky way-like galaxies. When our results are far from the values presented in this table, most likely the results are unphysical.

Component	Parameter Range	Units
Bulge I	$a = 0$	$kpc$
	$0.0 < b < 0.5$	$kpc$
	$0.1 < M < 1.0$	$10^{10}M_{\odot}$
Bulge II	$0.01 < a < 0.05$	$kpc$
	$0.5 < b < 1.5$	$kpc$
	$1 < M < 5$	$10^{10}M_{\odot}$
Thin Disc	$1 < a < 10$	$kpc$
	$0.1 < b < 1.0$	$kpc$
	$0.5 < M < 1.5$	$10^{11}M_{\odot}$
Thick Disc	$1 < a < 10$	$kpc$
	$0.1 < b < 15.0$	$kpc$
	$0.5 < M < 1.5$	$10^{11}M_{\odot}$
Exponential Disc	$2 < h_r < 6$	$kpc$
	$1 < \Sigma_0 < 15$	$10^2M_{\odot}/pc^2$
NFW - Halo	$0.1 < a < 30$	$kpc$
	$0.1 < M_0 < 10$	$10^{11}M_{\odot}$
Burkert - Halo	$2 < a < 38$	$kpc$
	$0.1 < \rho_0 < 10$	$10^6M_{\odot}/kpc^3$

txt file containing three columns: the radial coordinate (in kpc units), the circular velocity and its uncertainty (in km/s).

### 3.2. GalRotpy panel

**GalRotpy** panel is composed by two blocks which are shown in Fig. 6. The left block (Fig. 6—left) includes a checklist to select the available potentials to model the rotation curve, it also includes a set of sliders for each mass contribution and scale parameters with identifiable colors. The sliders present a red guide showing the resulting fit values for each parameter or the default values described in the previous subsection. Finally, there are two buttons: to reset all the parameters to their input values, and to start the parametric fit process.

The right block (Fig. 6—right) shows the composed rotation curve given by the black solid line, the different potentials selected to reproduce the data and the reduced  $\chi^2$  which is written as

$$\chi^2 = \frac{1}{N_{dof}} \sum_{i=1}^N \left[ \frac{v_i^{data} - v_i^{model}}{v_i^{error}} \right]^2, \quad (27)$$

where  $N_{dof} = N - N_{dim}$  represents the system's degrees of freedom, defined in terms of the number of data points  $N$  and the number of parameter being used  $N_{dim}$  (hereafter known as the system's dimension). Here, the equation (27) provides to the user a notion of how good the fit is ( $\chi^2 \approx 1$ ), which also helps to decide which profiles are a good match for the input rotation curve.

Each potential is represented by a dashed line identified by a color. These rotations curves are obtained by using galpy, which is a python library that contains a set of tools for galactic dynamics, including gravitational potentials and its derived quantities: mass density, circular velocity, total mass, among others. galpy performs numerical orbit integration with a variety of Runge–Kutta-type and symplectic integrators; and it supports the calculation of action-angle coordinates and orbital frequencies for spherical potentials. It includes some distribution functions (DF) also like two-dimensional axisymmetric and non-axisymmetric disc DFs, a three-dimensional disc DF, and a DF framework for tidal streams Bovy (2015).

For more details about how galpy works please refer to

Bovy (2015) and its corresponding documentation<sup>2</sup>.

### 3.3. Fitting process and output

The **GalRotpy** visual interface is a great help when the behavior of rotation curves wants to be understood or explained, but even though the visual inspection of the different potentials allows the user to choose the best candidates to reproduce the data, and a set of parameters which at first glance seems to be correct, it is essential to find a better estimation of the parameters with their uncertainties.

To solve this problem we make use of the package emcee Foreman-Mackey et al. (2013) which implements a particular Markov chain Monte Carlo (MCMC) algorithm proposed by Goodman and Weare (2010), where instead of getting a best fit curve like a frequentist approach does, MCMC obtains the posterior probability distribution  $P(\Theta|\mathcal{D}, \mathcal{M})$  equation (28) with  $\Theta$ ,  $\mathcal{D}$  and  $\mathcal{M}$  being the parameters involved, the data used and the model (composed rotation curve in our case) respectively, such that

$$P(\Theta|\mathcal{D}, \mathcal{M}) = \frac{P(\mathcal{D}|\Theta, \mathcal{M})P(\Theta|\mathcal{M})}{P(\mathcal{D}|\mathcal{M})}, \quad (28)$$

where  $\mathcal{L} := P(\mathcal{D}|\Theta, \mathcal{M})$  is the likelihood,  $\Pi := P(\Theta|\mathcal{M})$  is the prior, and  $Z := P(\mathcal{D}|\mathcal{M})$  is the evidence (also known as marginal likelihood or normalization factor). Nevertheless, since the evidence is not considered in MCMC algorithms, we only need to input the likelihood and the prior distributions: for the likelihood we use a Gaussian distribution

$$\mathcal{L} \propto \exp \left( -\frac{1}{2} \sum_{i=1}^N \left[ \frac{v_i^{data} - v_i^{model}}{v_i^{error}} \right]^2 \right), \quad (29)$$

meanwhile as the prior we use the following step-like distribution

$$\Pi = \begin{cases} 1 & \text{if } \theta > 0 \\ 0 & \text{if } \theta \leq 0 \end{cases}, \quad (30)$$

where  $\theta$  refers to all parameters. It is worth noting that we chose this simple distributions (30) in order to not to give several constraints during the fitting process since we lack of information of how the different contributions to the composed circular velocity will adapt to the given data. In that case, there is previous knowledge which helps to constrain the parameters, it may be introduced into the probability distributions. For a further discussion about how to implement emcee please refer to its documentation<sup>3</sup>.

Now, regarding to how **GalRotpy** works, for each distribution we allow to their parameters to evolve only in a constrained way, due to the probability distribution given above; except for the bulge which can be modeled by means of two distributions: a spherical symmetric distribution or spheroidal distribution. The first one is described by means of the Plummer potential, which is achieved leaving  $a = 0$  kpc as initial guess such that this parameter will not be used through the fitting process. However, if the user let  $a > 0$  kpc as initial guess, the bulge will be modeled by means of the Miyamoto-Nagai potential.

Therefore, once the potentials (and also its parameters' values which seems to reproduce the data) have been chosen, the user is allowed to click on the start button. That closes the panel and it will start the fitting process. Then on the terminal- shell where **GalRotpy** script was launched, is shown the dimension of the system (number of parameters consider in total) and then the command shell prompt asks to introduce the number of walkers (Markov chains) to be used. The number of walkers must be an even number at least, twice the dimension. After that, the number of steps the user wants the walkers to take, has to be introduced in order to explore the parameters space.

An initial set of parameters or initial guess is needed for emcee to

<sup>2</sup> See <https://galpy.readthedocs.io/en/v1.4.0>.

<sup>3</sup> See <http://dfm.io/emcee/current>.

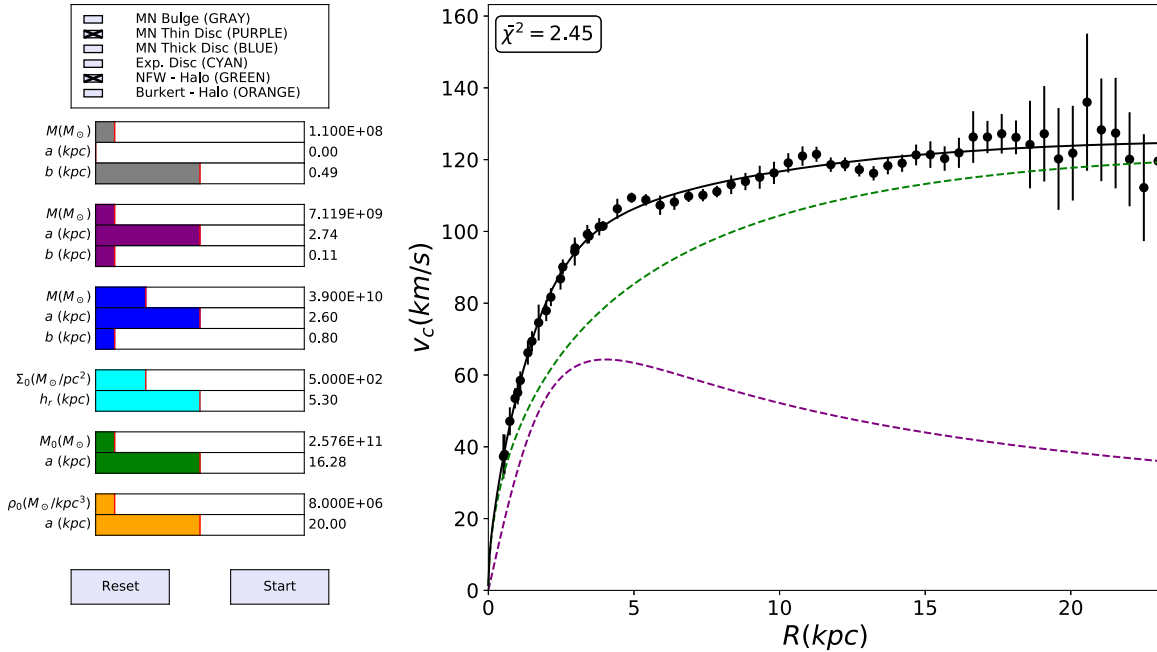


**Fig. 6.** Panel for gravitational potentials selection and parametrization (top) and its composed rotation curve with the corresponding contributions selected (bottom).

work, thus, such set corresponds to those parameters approximated through the visual fitting and are saved in a file named `init_guess_params.txt`. This initial guess needs to reproduce the data as well as possible, otherwise the results are more likely to diverge.

The success of the fitting process is linked to how well the walkers behave, such that it is advised to take a big enough number of steps for a small number of walker (at least twice the dimension of the system). So, the user can verify what combination of components are the best for the rotation curve to be studied along with checking if the walkers actually converge. If they do, the user can check whether they converge to physical values or not. Therefore, once one is sure which components to use and how well the walkers behave, in order to improve the estimation of the parameters, the fitting process can be run several times, each one using the very same input number of walkers and steps, making a new initial guess each time from half of the steps, thus the system evolves smoothly. If the user wants to run the process more than once, in the last run the walkers will take three times the number of input steps in order to have a better visualization of the walkers' behavior.

It is worth to notice that not for every possible combination of contributions **GalRotpy** will provided reliable results, since for some combination the walkers will diverge or converge to non physical values. This problem may be addressed using a careful number of steps (small compared to the number of steps by which the walkers start to diverge) and running **GalRotpy** as many times as considered correct. Nevertheless this procedure most of the times yields to non physical results, so it must be applied carefully.

After the walkers explore the parameters' space (fitting process), a window opens. Such window shows the walkers behavior (Markov chains) as it is shown in Fig. 7. This window has three buttons: two of them allow the user to see the samples for each parameter being studied so, that it is easy to determine from which step the chains are actually converging. It means that it is possible to get rid of those steps which are not useful; for example in Fig. 7 the fact of getting rid of the first 500 steps, gives excellent results. Hence, when the user decides how many steps to burn in, after clicking on the named button, the window closes and the number of steps to be burn in, has to be introduced in the terminal- shell.

Finally, this leads to three files: the first one is a text file named

`final_params.txt` which includes the parameters' values obtained with their corresponding uncertainties for the 68% and 95% quantiles, and two plots: one shows the curve obtained with each of the contributions used, and the other one shows the credibility regions which are plotted using the package `corner` Foreman-Mackey (2016)<sup>4</sup>. In regards to the credibility, as can be seen in Fig. 10 and Fig. 11 we have that, the inner dark region corresponds to the 68% likelihood, followed by a fainter region corresponding to the 95% likelihood. The outer dark dotted region corresponds to the data beyond the 95% likelihood.

In case that the exponential disc is selected, the text file `final_params.txt` will also include the total mass of the given disc  $M_d$ , likewise, for both dark halos it will also be included the concentration parameter  $X$  and the halo's total mass  $M_h$  for a given cosmological overdensity  $\Delta_c$ . Last but not least, it is included the reduced  $\chi^2$  for the best fit, which corresponds to the set of parameters that maximize (29). Since these quantities are not included directly along the fitting process, they will not appear in the credibility regions plot.

#### 4. Results using GalRotpy

For the purpose of showing how **GalRotpy** works, we use the disc galaxies M33 and NGC6361 as test cases to find a dynamical model that describes approximately the gravitational potential of the given galaxies. For M33 we are able to compare our results with those reported by López Fune et al. (2017).

##### 4.1. NGC6361 test case

To get the rotation curve of NGC6361, we first make a selection of some galaxies from CALIFA (Calar Alto Legacy Integral Field Area) survey, which provides data cubes of more than 600 galaxies in the local universe with  $0.005 < z < 0.03$ . CALIFA survey uses Integral Field Spectroscopy (IFS) to integrate the properties of images and spectroscopy. The data cubes have information about kinematic properties from emission and absorption lines, stellar populations, and other physical features of each galaxy in CALIFA survey sample García-Benito

<sup>4</sup> See <https://corner.readthedocs.io/en/latest/>.

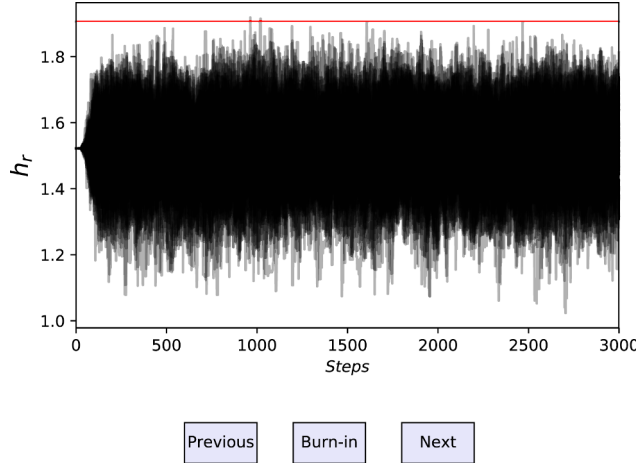


**Fig. 7.** Panel to explore walkers' behavior for each parameter being considered. This particular example presents the behavior of  $h_r$  for the fitting process shown in Fig. 11 (top). The red line represents the corresponding initial guess value obtained by means of the visual inspection (fit).

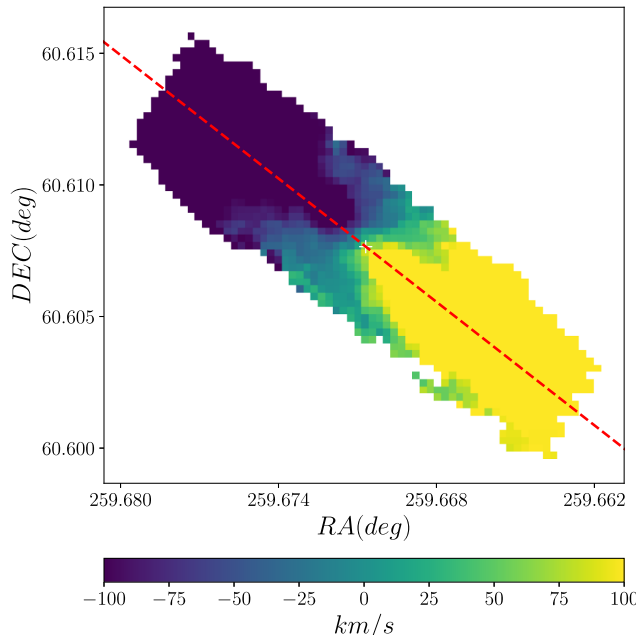


**Fig. 8.** Gas velocity field of NGC6361 for the data product, provided by CALIFA collaboration. X and Y axis indicates right ascension (RA) and declination (DEC) respectively. The red line represents the major axis of the system.

et al. (2015). Then, we select the NGC6361 galaxy which is a spiral galaxy type (SA $b$  edge-on) that does not present a bar-like structure in it<sup>5</sup>. After that, we obtain from CALIFA survey the data product of NGC6361, one derived using PIPE3D, a technique implemented by Sánchez et al. (2016). Based on the datacube of NGC6361 and the velocity map for H $\alpha$  emission line provided by CALIFA collaboration, we get the Fig. 8.

In this example, the rotation curve of NGC6361 is obtained from the points over the kinematic center, taken over the radial coordinate on the gas velocity field, along the given major axis (see Fig. 8). To accomplish this task, we have defined two coordinate systems, each one with respect to a given plane: one of them is perpendicular to the line of sight, while the other is perpendicular to the galaxy's polar axis, such

<sup>5</sup> See <http://simbad.u-strasbg.fr/simbad/sim-basic?Ident=ngc6361submit=SIMBAD+search>.

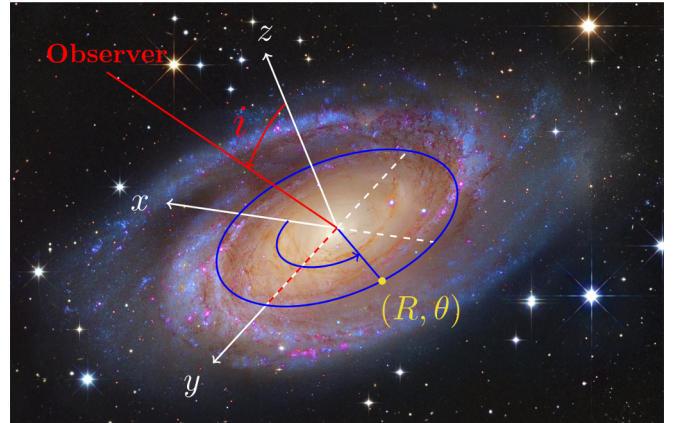


**Fig. 9.** Set up used to derive the rotation curve from observations. At the top we have the trajectory (blue curve) followed by a star (yellow point) with polar coordinates  $(R, \theta)$ , with respect to the galaxy's coordinate system. We can see that the galaxy is inclined with respect to the observer's line of sight (red) by an angle  $i$ . At the bottom we have the representation of a trajectory as it is seen in the galaxy's plane (left) and in the observer's plane (right) with their respective polar coordinates, where it has been considered that the axis  $x$  and  $\bar{x}$  are parallel along the major axis. The galaxy used in this illustration (top) corresponds to the spiral galaxy M81 (see <https://apod.nasa.gov/apod/ap141119.html>), whose credits are: Image Credit: Subaru Telescope, Hubble Space Telescope. Processing and Copyright: Roberto Colombari and Robert Gendler.

that the inclination angle between these planes is named  $i$ ; see Fig. 9 (top). Thus, if we set these coordinate systems in such a way that the axis  $x$  and  $\bar{x}$  are parallel, and coincide with the galaxy's major axis as seen by the observer, we can relate the position of a star over the galaxy's plane and the observer's plane, as it is illustrated in Fig. 9 (bottom).

Consider a point (star) in the galaxy's plane, with position  $(R, \theta)$  (see Fig. 9 bottom-left), and whose velocity in this coordinate basis is

$$\mathbf{V}_\star = (V_R \cos(\theta) - V_\theta \sin(\theta))\hat{x} + (V_R \sin(\theta) + V_\theta \cos(\theta))\hat{y}.$$

Now, the observer is capable of measuring only the component of the velocity along its line of sight i.e., along  $\bar{z}$ , which is given by  $\bar{z} \cdot \mathbf{V}_\star$ . Therefore, taking into account that from our set up the relations  $\hat{x} = \bar{x}$ , and  $\hat{y} = \cos(i)\bar{y} + \sin(i)\bar{z}$ , are satisfied, the velocity measured by the observer turns out to be Beckman et al. (2004)

$$V_{obs} = V_{sys} + V_\theta \sin(i) \cos(\theta) + V_R \sin(i) \sin(\theta). \quad (31)$$

Here, an additional term named systemic velocity ( $V_{sys}$ ) is added, which corresponds to the velocity of the galaxy as a whole (given by the spectroscopic redshift), while  $V_R$  and  $V_\theta$  represent the velocity along the radial and tangential direction respectively; with  $V_\theta$  being the velocity component we are interested in. For this situation is commonly assumed that  $V_R$  can be neglected, and also, for simplicity only the velocities along the major axis are considered ( $\theta = 0$ ). Then, from (31) the circular velocity reads

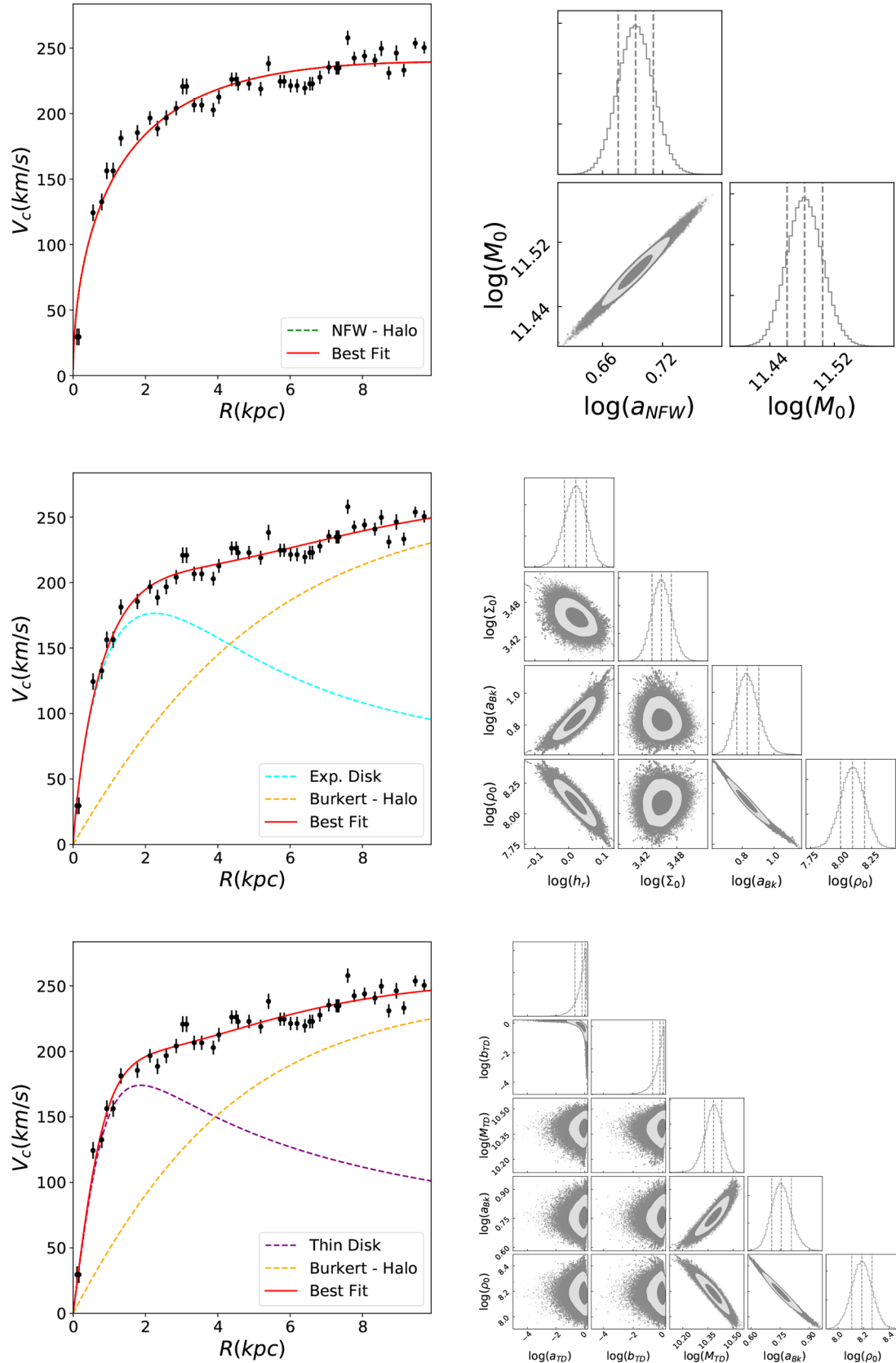


**Fig. 10.** Rotation curve (left) and credibility regions (right) for three different models which attempt to reproduce the rotation curve of the disc galaxy NGC6361. The models are: NFW dark halo (top), Burkert dark halo + Exponential disk (middle) and Burkert dark halo + Thin disk (bottom).

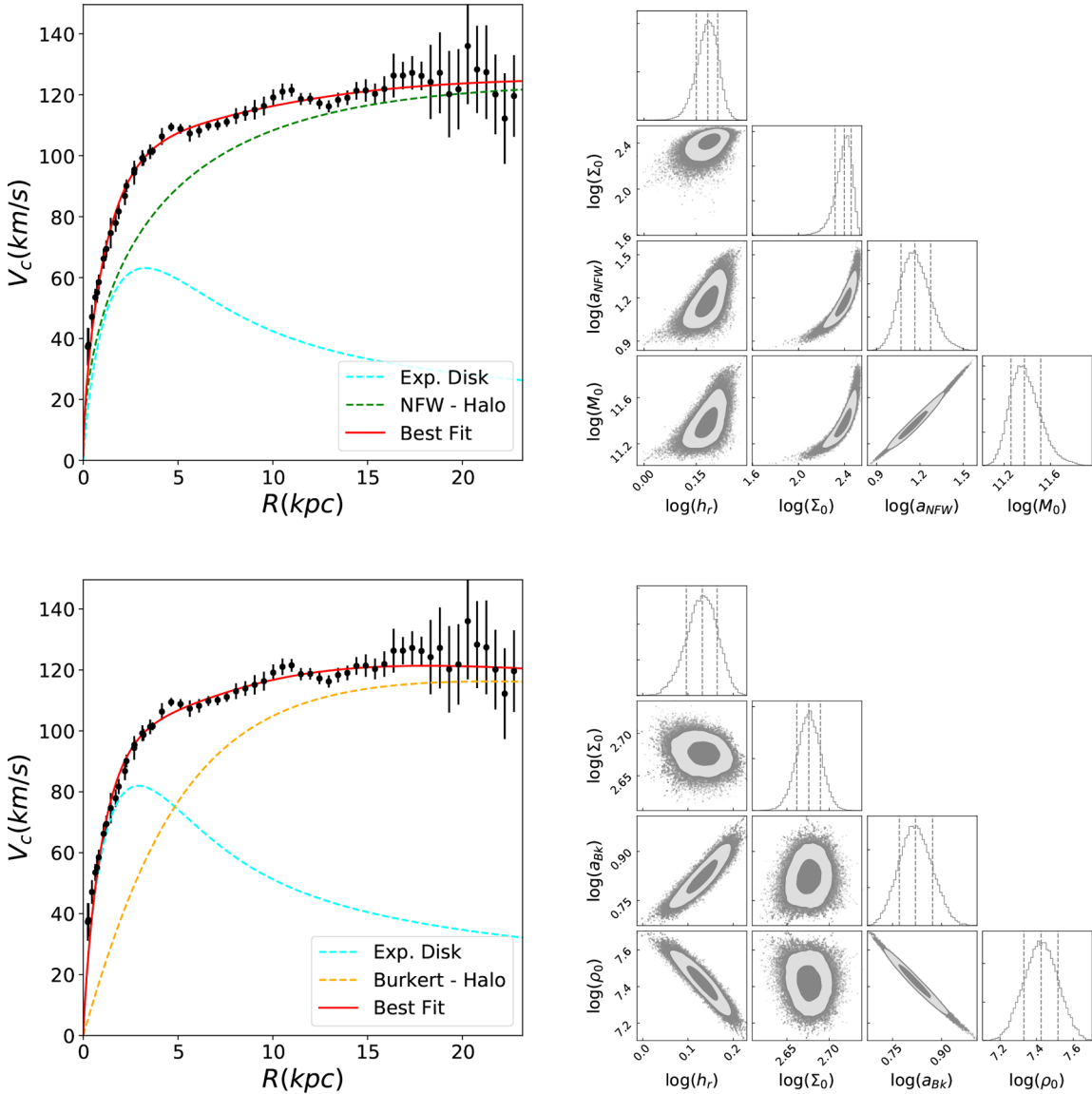


**Fig. 11.** Rotation curve (left) and credibility regions (right) for two different models which attempt to reproduce the rotation curve of the disc galaxy M33. The models are: NFW dark halo + Exponential disk (top) and Burkert dark halo + Exponential disk (bottom). The rotation curve was taken from Corbelli et al. (2014).

$$V_\phi = \frac{V_{\text{obs}} - V_{\text{sys}}}{\sin(i)}. \quad (32)$$

In this case, we have assumed that the gas velocity follows approximately the galaxy potential like the stars velocity field.

At this point we have described how it is possible to obtain the rotation curve (32) from observations, therefore, from now on we will focus on the analysis of this curve using **GalRotpy**.

In the literature is often found that for a given value of  $\Delta_c$ , dark halos contributions are parametrized directly through its total mass  $M_h$  and the concentration parameter  $X$ ; mostly the NFW profile. However, although **GalRotpy** does not use this parameters to fit the rotation curve, they can be derived as it is discussed in section 2.3.5, while the total mass  $M_*$  corresponding to the exponential disk is easily calculated by using (12).

Therefore, from its rotation curve, now it is possible to characterize NGC6361. Here, we show three models which provide reliable

parameters' values (see Table 2), where we run the fit process twice for 100 walkers, 3000 steps and  $\Delta_c = 97.2$ .

We modeled this galaxy's rotation curve using both dark matter halo profiles available in **GalRotpy**. For the NFW profile we found that reliable results are obtained only when this profile is applied, whose rotation curve is shown in Fig. 10 (top). It means that this profile is capable of reproducing the rotation curve by itself, which suggests that within the corresponding uncertainties, NGC6361 is a galaxy dominated by dark matter, for a halo with a mass  $M_h \sim 10^{12} M_\odot$  concentrated within a radius  $r_c \sim 10^2 \text{kpc}$ . On the other hand, for the Burkert profile, we found that it is not capable of reproducing the given rotation curve by itself, which is expected considering its behavior (see Fig. 5), since this profile cannot reproduce the cusp in the inner region. We obtained two models compatible with the data, each one for a different disk profile: an exponential disk (Fig. 10 - middle) and a thin disk (Fig. 10 - bottom). Such disks structures are dominant in the inner regions,

**Table 2**

Set of parameters obtained using **GalRotpy** with their corresponding uncertainties for three different models for the rotation curve of NGC6361. For each dark halo distribution, the halo's total mass  $M_h$  and the concentration parameter  $X$  are given for  $\Delta_c = 97.2$ .

Model I				
Component	Parameter	Fit	68%	95%
NFW-Halo	$a(kpc)$	4.93	$+0.21$	$+0.42$
	$M_0(\times 10^{11}M_\odot)$	3.04	$+0.16$	$+0.33$
	$\rho_0(\times 10^8 M_\odot/kpc^3)$	2.02	$-0.15$	$-0.28$
	$X(\times 10)$	5.27	$+0.15$	$+0.31$
	$M_h(\times 10^{11}M_\odot)$	9.14	$-0.14$	$-0.27$
Model II				
Exponential Disc	Parameter	Fit	68%	95%
	$h_r(kpc)$	1.05	$+0.08$	$+0.15$
	$\Sigma_0(\times 10^3 M_\odot/pc^2)$	2.84	$+0.11$	$+0.22$
	$M_\star(\times 10^{10}M_\odot)$	1.97	$-0.11$	$-0.23$
Burkert-Halo	$a(kpc)$	6.79	$+1.25$	$+2.21$
	$\rho_0(\times 10^8 M_\odot/kpc^3)$	1.24	$+0.32$	$+0.69$
	$X(\times 10)$	4.51	$+0.37$	$+0.81$
	$M_h(\times 10^{12}M_\odot)$	1.49	$-0.40$	$-0.70$
Model III				
Thin Disc	Parameter	Fit	68%	95%
	$a(\times 10^{-1}kpc)$	6.56	$+4.48$	$+6.58$
	$b(\times 10^{-1}kpc)$	6.64	$+4.46$	$+6.58$
	$M_\star(\times 10^{10}M_\odot)$	2.42	$-4.49$	$-6.30$
Burkert-Halo	$a(kpc)$	5.70	$+0.73$	$+1.62$
	$\rho_0(\times 10^8 M_\odot/kpc^3)$	1.53	$+0.31$	$+0.68$
	$X(\times 10)$	4.87	$-0.26$	$-0.47$
	$M_h(\times 10^{12}M_\odot)$	1.11	$+0.35$	$+0.71$

**Table 3**

Set of parameters obtained using **GalRotpy** with their corresponding uncertainties for two models for the rotation curve of M33. For each dark halo distribution the halo's total mass  $M_h$  and the concentration parameter  $X$  are given for  $\Delta_c = 97.2$ .

Model I				
Component	Parameter	Fit	68%	95%
Exponential Disc	$h_r(kpc)$	1.52	$+0.10$	$+0.20$
	$\Sigma_0(\times 10^2 M_\odot/pc^2)$	2.50	$+0.37$	$+0.66$
	$M_\star(\times 10^9 M_\odot)$	3.61	$-0.43$	$-0.90$
NFW-Halo	$a(\times 10 kpc)$	0.96	$+0.96$	$+1.89$
	$M_0(\times 10^{11} M_\odot)$	1.46	$-0.29$	$-0.49$
	$\rho_0(\times 10^6 M_\odot/kpc^3)$	2.37	$+0.91$	$+2.45$
	$X(\times 10)$	6.05	$-0.55$	$-0.91$
	$M_h(\times 10^{11} M_\odot)$	1.37	$+2.96$	$+6.88$
Model II				
Exponential Disc	Parameter	Fit	68%	95%
	$h_r(kpc)$	4.16	$+0.24$	$+0.48$
	$\Sigma_0(\times 10^2 M_\odot/pc^2)$	2.05	$-0.22$	$-0.42$
	$M_\star(\times 10^9 M_\odot)$	1.11	$+1.11$	$+2.86$
Burkert-Halo	$a(kpc)$	6.61	$+0.84$	$+1.71$
	$\rho_0(\times 10^7 M_\odot/kpc^3)$	2.66	$+0.63$	$+1.32$
	$X(\times 10)$	2.52	$-0.52$	$-0.89$
	$M_h(\times 10^{11} M_\odot)$	2.39	$+0.22$	$+0.43$

approximately  $R < 4kpc$ , beyond this limit in both cases the disc contribution starts decreasing rapidly and the dark halo is the dominant dynamical component. For this profile, we also found that within the corresponding uncertainties the dark halo is dominant with a mass  $M_h \sim 10^{12} M_\odot$  enclosed within a radius  $r_c \sim 10^2 kpc$  with respect to a mass  $M_\star \sim 10^{10} M_\odot$  for the disc contribution.

#### 4.2. M33 test case

We now focus on M33 which is a spiral galaxy type (SA(s)cd, Face-on) without a bar-like structure<sup>6</sup>. We will characterize this galaxy based on the rotation curve taken from Corbelli et al. (2014), such that following López Fune et al. (2017), we have two models: in both cases we use an exponential disc potential to model the stellar and gaseous contribution, while the dark halo is modeled through NFW and Burkert profiles.

Here, for both models we have a system of six dimensions (parameters) where we run the fit process twice for 100 walkers, 1000 steps and  $\Delta_c = 97.2$  López Fune et al. (2017). Each parameter being considered converge as shown in Fig. 7, such that the models are well adapted to the data. The parameters obtained are presented in Table 3, which within the corresponding uncertainties agree with those reported in López Fune et al. (2017), presented in Table 4.

From Fig. 11 we can see that beyond  $R \approx 5kpc$  for both models, the dark halo is the dominant contribution, and it rules the dynamics of the stars at this radius. However, the NFW profile presents a more significant contribution for the dynamics in the inner region, producing a more massive halo than the Burkert profile in Model II. On the other

hand, since the Burkert profile is not capable of reproducing the cusp presented in the inner region ( $R < 5kpc$ ), thus, to compensate this fact the exponential disc turns out to be more massive than it is in Model I, then the baryonic matter is dominant in the inner region.

#### 5. Conclusions

In this paper we have presented **GalRotpy**, which is a tool for the real-time composition of rotation curves of disc-like galaxies, being a straightforward and powerful method to study the behavior of rotation curves. This method gives an approximation to the dynamics of stellar systems and its global gravitational features. Thus, **GalRotpy** allows the user to check the presence of an assumed mass type component in an observed rotation curve, by including or removing a mass model quickly, then by means of a MCMC parametric fit, it is possible to verify if in fact, the contributions chosen are compatible with the data. From this fit process **GalRotpy** provides an estimation of the parameters involved with their uncertainties within the 68% and 95% likelihood, along with a plot of the credibility regions associated to the intrinsic parameters of each contribution applied (those associated to the different profiles), by which it is easy to infer the main mass contribution quantitatively, in a galaxy from the mass ratios between pairs of mass components. Especially the bulge to disc and, the disc to dark matter halo ratios are relevant. **GalRotpy** also provides a plot which includes the composed rotation curve and its corresponding contributions, so it is possible to study qualitatively the influence of each component to the dynamics of the stellar system.

In order to present the capabilities of **GalRotpy** we have performed the analysis for the disc galaxies NGC6361 and M33. For NGC6361 we found three models consistent with the data: when the dark halo was modeled with the NFW profile, we obtained that this profile by itself is capable of reproducing the rotation curve, suggesting that the dark halo is the dominant dynamical component for this galaxy. Nevertheless, when the dark halo was modeled with the Burkert profile unlike the foregoing model, since the Burkert profile is not capable of reproducing the inner cusp of this rotation curve, the presence of an additional structure was essential. For this task, we added a disc structure using an exponential disc and also a thin disc, such that in either case we have that the dynamical

<sup>6</sup> See <http://simbad.u-strasbg.fr/simbad/sim-basicIdent=m33submit=SIMBAD+search>.

**Table 4**Set of parameters reported by López Fune et al. (2017). Here  $\Delta_c = 97.2$ .

Model I			
Component	Parameter	Fit	Uncertainty
Stellar-Gas-Halo	$M_*( \times 10^9 M_\odot)$	4.9	$\pm 1.5$
NFW-Halo	$M_h( \times 10^{11} M_\odot) X$	5.4 9.5	$\pm 0.6 \pm 0.7$
Model II			
Component	Parameter	Fit	Uncertainty
Stellar-Gas-Halo	$M_*( \times 10^9 M_\odot)$	4.9	$\pm 1.5$
Burkert-Halo	$a(kpc)\rho_0( \times 10^6 M_\odot/kpc^3)M_h( \times 10^{11} M_\odot)$	9.5 12.3 3.0	$\pm 0.6 \pm 1.0 \pm 0.8$

behavior in the inner region (approximately  $R < 4kpc$ ) is dominated by the disc structure. With respect to M33 we applied the models suggested in López Fune et al. (2017), where our results are qualitatively and quantitatively in agreement with what they have reported.

### Declaration of competing interest

The authors declare that they have no known competing financial interests or personal relationships that could have appeared to influence the work reported in this paper.

### Acknowledgements

We thank PhD Jorge Barrera-Ballesteros and PhD Sebastián Sánchez for their collaboration on generating the kinematic map of NGC6361 from CALIFA survey. In the same way, we thank PhD E. López Fune, PhD P. Salucci and PhD E. Corbelli by allow us to use the rotation curve data of M33 galaxy. We are grateful to PhD P. Salucci for their suggestions on using the Burkert profile, giving broad capabilities to GalRotpy for building rotation curves of disc-like galaxies.

### References

- Ade, P.A., Aghanim, N., Arnaud, M., Ashdown, M., Aumont, J., Baccigalupi, C., Banday, A., Barreiro, R., Bartlett, J., Bartolo, N., et al., 2016. Planck 2015 results-xiii. cosmological parameters. *Astronomy & Astrophysics* 594, A13.
- Babcock, H.W., 1939. The rotation of the andromeda nebula. *Lick Observatory Bulletin* 19, 41–51.
- Beckman, J.E., Zurita, A., Vega Beltrán, J.C., 2004. Kinematic measurements of gas and stars in spiral galaxies. *Lecture Notes and Essays in Astrophysics* 1, 43–62.
- Binney, J., Tremaine, S., 2011. Galactic dynamics. 20 Princeton university press.
- Bovy, J., 2015. galpy: A python library for galactic dynamics. *The Astrophysical Journal Supplement Series* 216 (2), 29.
- Bryan, G.L., Norman, M.L., 1998. Statistical properties of x-ray clusters: Analytic and numerical comparisons. *The Astrophysical Journal* 495 (1), 80.
- Burkert, A., 1995. The structure of dark matter halos in dwarf galaxies. *The Astrophysical Journal Letters* 447 (1), L25.
- Coe, D., 2010. Dark matter halo mass profiles. arXiv preprint arXiv:1005.0411.
- Corbelli, E., Thilker, D., Zibetti, S., Giovanardi, C., Salucci, P., 2014. Dynamical signatures of a  $\Lambda$ cdm-halo and the distribution of the baryons in m 33. *Astronomy & Astrophysics* 572, A23.
- Cuddeford, P., 1993. On the potentials of galactic discs. *Monthly Notices of the Royal Astronomical Society* 262 (4), 1076–1086.
- Foreman-Mackey, D., 2016. corner.py: Scatterplot matrices in python. *The Journal of Open Source Software* 24. <https://doi.org/10.21105/joss.00024>.
- Foreman-Mackey, D., Hogg, D.W., Lang, D., Goodman, J., 2013. emcee: the mcmc hammer. *Publications of the Astronomical Society of the Pacific* 125 (925), 306.
- Freeman, K.C., 1970. On the disks of spiral and s0 galaxies. *The Astrophysical Journal* 160, 811.
- García-Benito, R., Zibetti, S., Sánchez, S., Husemann, B., De Amorim, A., Castillo-Morales, A., Fernandes, R.C., Ellis, S., Falcón-Barroso, J., Galbany, L., et al., 2015. Califa, the calar alto legacy integral field area survey-iii. second public data release. *Astronomy & Astrophysics* 576, A135.
- Goodman, J., Weare, J., 2010. Ensemble samplers with affine invariance.
- Communications in applied mathematics and computational science 5 (1), 65–80.
- Jimenez, R., Verde, L., Oh, S.P., 2003. Dark halo properties from rotation curves. *Monthly Notices of the Royal Astronomical Society* 339 (1), 243–259.
- Karukas, E.V., Salucci, P., 2016. The universal rotation curve of dwarf disc galaxies. *Monthly Notices of the Royal Astronomical Society* 465 (4), 4703–4722.
- Kuzmin, G., 1956. Model of the steady galaxy allowing of the triaxial distribution of velocities. *Astron. zh* 33, 27.
- López Fune, E., Salucci, P., Corbelli, E., 2017. Radial dependence of the dark matter distribution in m33. *Monthly Notices of the Royal Astronomical Society* 468 (1), 147–153.
- Miyamoto, M., Nagai, R., 1975. Three-dimensional models for the distribution of mass in galaxies. *Publications of the Astronomical Society of Japan* 27, 533–543.
- Mo, H., Van den Bosch, F., White, S., 2010. Galaxy formation and evolution. Cambridge University Press.
- Navarro, J.F., Frenk, C.S., White, S.D., 1997. A universal density profile from hierarchical clustering. *The Astrophysical Journal* 490 (2), 493.
- Noordermeer, E., Van Der Hulst, J., Sancisi, R., Swaters, R., Van Albada, T., 2007. The mass distribution in early-type disc galaxies: declining rotation curves and correlations with optical properties. *Monthly Notices of the Royal Astronomical Society* 376 (4), 1513–1546.
- Oort, J.H., 1940. Some problems concerning the structure and dynamics of the galactic system and the elliptical nebulae ngc 3115 and 4494. *Astrophysical Journal* 91.
- Persic, M., Salucci, P., Stel, F., 1996. The universal rotation curve of spiral galaxies - i. the dark matter connection. *Monthly Notices of the Royal Astronomical Society* 281 (1), 27–47.
- Plummer, H.C., 1911. On the problem of distribution in globular star clusters. *Monthly notices of the royal astronomical society* 71, 460–470.
- Pouliasis, E., Di Matteo, P., Haywood, M., 2017. A milky way with a massive, centrally concentrated thick disc: new galactic mass models for orbit computations. *Astronomy & Astrophysics* 598, A66.
- Rubin, V.C., Ford Jr, W.K., 1970. Rotation of the andromeda nebula from a spectroscopic survey of emission regions. *The Astrophysical Journal* 159, 379.
- Rubin, V.C., Ford Jr, W.K., Thonnard, N., 1980. Rotational properties of 21 sc galaxies with a large range of luminosities and radii, from ngc 4605 ( $r=4kpc$ ) to ugc 2885 ( $r=122kpc$ ). *The Astrophysical Journal* 238, 471–487.
- Salucci, P., Burkert, A., 2000. Dark matter scaling relations. *The Astrophysical Journal Letters* 537 (1), L9.
- Samurovic, S., 2007. Dark matter in elliptical galaxies. *Publications de l'Observatoire Astronomique de Beograd* 81.
- Sánchez, S., Pérez, E., Sánchez-Blázquez, P., García-Benito, R., Ibarra-Medina, H., González, J., Rosales-Ortega, F., Sánchez-Menguiano, L., Ascasíbar, Y., Bitsakis, T., et al., 2016. Pipe3d, a pipeline to analyze integral field spectroscopy data: ii. analysis sequence and califa dataproducts. *Revista mexicana de astronomía y astrofísica* 52 (1), 171–220.
- Sanders, R.H., 2010. The dark matter problem: a historical perspective. Cambridge University Press.
- Slipher, V.M., 1914. The detection of nebular rotation. *Lowell Observatory Bulletin* 2, 66.
- Sofue, Y., 1996. The most completely sampled rotation curves for galaxies. *The Astrophysical Journal* 458, 120.
- Sofue, Y., 2016. Rotation curve decomposition for size–mass relations of bulge, disk, and dark halo components in spiral galaxies. *Publications of the Astronomical Society of Japan* 68 (1).
- Sofue, Y., Rubin, V., 2001. Rotation curves of spiral galaxies. *Annual Review of Astronomy and Astrophysics* 39 (1), 137–174.
- Toomre, A., 1963. On the distribution of matter within highly flattened galaxies. *The astrophysical journal* 138, 385.
- Zwicky, F., 1933. Die rotverschiebung von extragalaktischen nebeln. *Helvetica Physica Acta* 6, 110–127.
- Zwicky, F., 1937. On the masses of nebulae and of clusters of nebulae. *The Astrophysical Journal* 86, 217.